Applications of Interferometry

Matthew Cardozo
matthewcardozo012@berkeley.edu

April 9, 2019

Abstract

Interferometry is a family of observational techniques that provides us with some of the most precise wave form measurements. We have learned over the course of this lab that the super-positioning of waves help use constructive and destructive interference to our advantage, so as to pronounce features of the wave on to a fringe signal that would otherwise be distorted by noise. With a precise measurement of the fluctuations that characterize this fringe, we could deduce the distance between our interferometers and with that resolve the diameter of our source.

Accordingly, the objective of this paper was to lead an investigation into just how precise these measurements could be. We discovered that our interferometers had the capability of resolving a fringe for the Sun to about the nearest 100^{th} of a millivolt. This yielded measurements of the baseline components to a near one-millionth of a percent. Our resulting baseline values from the Sun data were $B_{ew} \approx 16.54$ meters and $B_{ns} \approx 0.97$ meters, whereas M17 data gave $B_{ew} \approx 17.19$ meters and $B_{ns} \approx 1.01$ meters. Altogether, we were able to calculate the Sun's angular diameter to be $\Theta_r = 0.289^\circ$, which was 15.6% off from our expected value of 0.25°. When expressing this as a circular diameter, our measurement was within 9% of the true value.

1 Introduction

There are two separate observations that are analyzed throughout this lab. The first is of the Sun, an extended source due to its close proximity to Earth. The second is M17, a nebula so far from Earth that it is considered a point source. The measurement of a fringe is therefore different in both cases. The fringe response associated with the Sun yielded a signal whose phase and amplitude fluctuated with the Sun's position in the sky, therefore a function of time. Due to the extended nature of the Sun and its corresponding fringe response, we were able to use the fluctuations in our fringe to deduce an angular diameter. The fringe response associated with M17 did not produce a similar fringe, but instead yielded a rather noisy signal of the sky in which we were forced to find our source. Additionally, we used both individual observations to track the movement of these sources across sky and calculate the relative baseline components of our interferometers.

Section 2 of this report concerns itself with the theory and applications of interferometry. Section 3 reviews our observed data, providing an in-depth analysis of the fringe signal and errors associated with our measurements. Section 4 is where we outline the steps necessary to both calculate the angular diameter of the Sun and measure appropriate values for the baseline components.

2 Interferometry

2.1 Background

Interferometry is a method of observation that uses the superposition of waves to reconstruct a new signal. One of the advantages of interferometry is the ability to simultaneously measure various signals from the same source. More interferometers allow for the observation of more signals, and the constructive and destructive interference of these signals is what returns a Fringe whose wave characteristics are expected to be more precise than those of the individually measured waves.

The interferometry technique we used in this lab was concerned with the superposition of two separately observed signals. Though collected from the same source, the signals were registered by two different interferometers - the superimposed signal represented the Fringe. Because the two interferometers differed in location with respect to the source, interference between the two signals occurred over a time delay that in result produced a Fringe whose phases and amplitudes varied as a function of the source's position on the sky.

2.2 Fringe Theory

The theory concerning the Fringe can be understood by first looking at the way in which the signals were initially collected. The interferometers atop of Campbell Hall used a parabolic dish that diffracted the incoming signals to one focal point. This process is what led to the interference between signals and yielded a wave whose form was a precise representation of the many recombined signals received from the source. Because this happened on both interferometers within a small time delay, the recombination of these two signals produced a wave that fluctuated as a function of the source's position on the sky. We recognized that the phases of our Fringe decreased as the source approached the zenith and increased as the source approached the horizon. This was expected since a signal received from the horizon would have to travel a larger distance to cover the space between the two interferometers - refer to Figure 1. Provided that the time delay was directly related to the distance between the interferometers, we aimed to extract the relative baseline distances from the information provided by the Fringe.

This concept of the Fringe is similar to those seen with the DSB mixer and the autocorrelation function. The DSB mixer combined signals by meeting our sampled signal with an LO whose frequency was slightly different that of our sample. This allowed us to use the mixer as a filter that passed only the reduced frequency that resulted from taking the difference of the two signals. The ACF was slightly different in that it combined two copies of the same signal, but with one slightly delayed with respect to the other. Much like the use of our interferometers, this allowed us to identify the similarities between the signals as a function of the time lag between them.

2.3 Representing the Fringe

Considering the relationship between the time lag and the distance over which the waves propagate, we sought to represent the Fringe as a function of baseline distance that varied with time. We began by expressing the components of our baseline with trigonometric functions of geometric time delay τ_g'.

$$F(h_s) = Acos(2\pi\nu\tau_g') + Bsin(2\pi\nu\tau_g') \tag{1}$$

We then chose to express our time delay as a function of h_s, the hour angle of the source that shifts with respect to the source's position in the sky. Recording in a UNIX time base allowed us to solve for the Julian Day as well as the position of the source in RA and DEC using *ugradio* coordinate module. These values were then used to obtain h_s and express our time delay in units of angular radians across the sky.

$$\nu\tau_g'(B_{ew}, B_{ns}, \delta, h_s) = [\frac{B_{ew}}{\lambda}cos(\delta)]sin(h_s) + [\frac{B_{ns}}{\lambda}sin(L)cos(\delta)]cos(h_s) \tag{2}$$

We defined the variables Q_{ew} and Q_{ns}, and in them absorbed the trigonometric components of our baseline that were with respect to the declination and latitude of our source.

$$Q_{ew} = [\frac{B_{ew}}{\lambda}cos(\delta)] \tag{3}$$

$$Q_{ns} = [\frac{B_{ns}}{\lambda}sin(L)cos(\delta)] \tag{4}$$

To develop an equation for the local Fringe frequencies, those of which change with h_s, we expanded the hour angle terms as Taylor series around the observed hour angle $h_{s,0}$. The result was an equation for the fringe frequencies in units of cycles per radian on the sky as shown below.

$$f_f = Q_{ew}cos(h_{s,0}) - Q_{ns}sin(h_{s,0}) \tag{5}$$

3 Observation

3.1 Getting the Data

The pointing segment of our script used the coordinate and interferometer modules from the *ugradio* package. We were able to guide the interferometers to point at the position in the sky where the source was located. We used a tracking time-step of 5 seconds that recorded data by the second. To ensure that our interferometers were correctly pointed, we had a raised exception that read 'Bad Pointing' if the pointed source was above or below the designated altitude and/or azimuth. Pointing at M17 was slightly different in that we had to use the precession module to account for its coordinates at the current equinox. The HP-Multimeter module was used to record and organize the data into individual lists titled 'Volts' and 'Times', making the extraction of the data much easier.

3.2 Sun Data

The data we collected from the Sun functioned as expected. Though we were unable to capture data from the horizon to the zenith, it is evident from Figure 1 that the fringe pattern was still very much present. We recorded two nulls in our data that occurred at the $1,420^{th}$ and $4,400^{th}$ second mark. By reading the way in which the patterns fluctuated, we were able to confirm that our observation began with the Sun near the horizon and progressed as the Sun rose towards the zenith. This was made clear by how the fringe phases increased as time progressed, signaling a decrease in the distance travelled between our two sampled waves. With incomplete data, we were forced in the analysis of the least-squares fitting to account for the possibility of mismatched zeros. This meant us having to cross check each of our zeros with the two present in our graph.

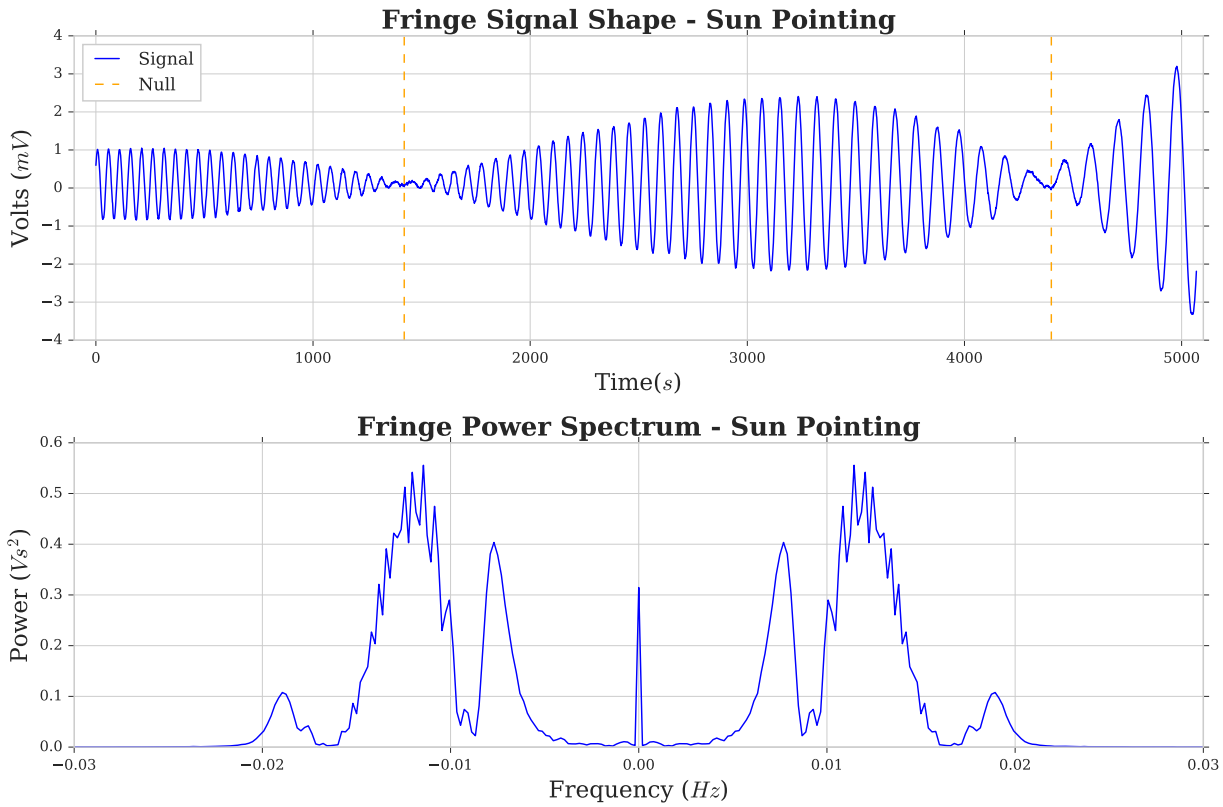

Figure 1: This figure shows our observation of the Sun. The top graph illustrates the fringe produced by our interferometers, and the bottom graph illustrates the power spectrum associated with this signal. Its clear in the fluctuation of our signal shape that the fringe is in fact present. This is attributed to the changing phase and amplitude of the wave. The larger phases correspond to the Sun being higher up in the sky, whereas the smaller phases correspond to the Sun being closer to the horizon.

The code below shows how our data was loaded in and used to solve for the frequencies and power of our signal from the Sun.

```
data = np.load('Sun_final.npz')
sun_data = data['volts'] * 1000
freq = np.fft.fftfreq(len(sun_data), d=1)
sun_pow = np.abs(np.fft.fft(sun_data)) ** 2 / 1e6
```

3.2.1 Errors in Sun Data

The errors in our Sun data were derived by constructing a list of the differences between adjacent data points. The following function illustrates how this was done:

```
def error(data):
    errors = []
```

```
for i in range(len(data) - 1):
    diff = data[i+1] - data[i]
    errors.append(diff)

last = np.mean(errors)
errors.append(last)
return errors
```

We plotted these errors in a normalized histogram and used *scipy.optimize* to fit a curve and try a range of standard deviations that best represented our data. According to this method, our data was measured to approximately $\frac{8}{100}^{th}$ of a mV, or more precisely 0.078 mV - refer to Figure 3.

3.3 M17 Data

On the contrary, the data we collected from M17 was quite difficult to work with. As shown in Figure 2, the data was heavily influenced by noise and showed fluctuations across the entire observation period. We expected our source to lie within the fraction of the signal that disobeyed the overall pattern of fluctuation. Our focus was drawn to around the $15,000^{th}$ second mark that displayed a rapid spike in the voltage of our signal. From our power spectrum of the signal we were also able to resolve 2 spikes, one of which we presumed to be our source. Because M17 was a point source rather than a circular source like the Sun, the inability of our interferometers to resolve an hour angle did not allow for any type of fringe pattern.

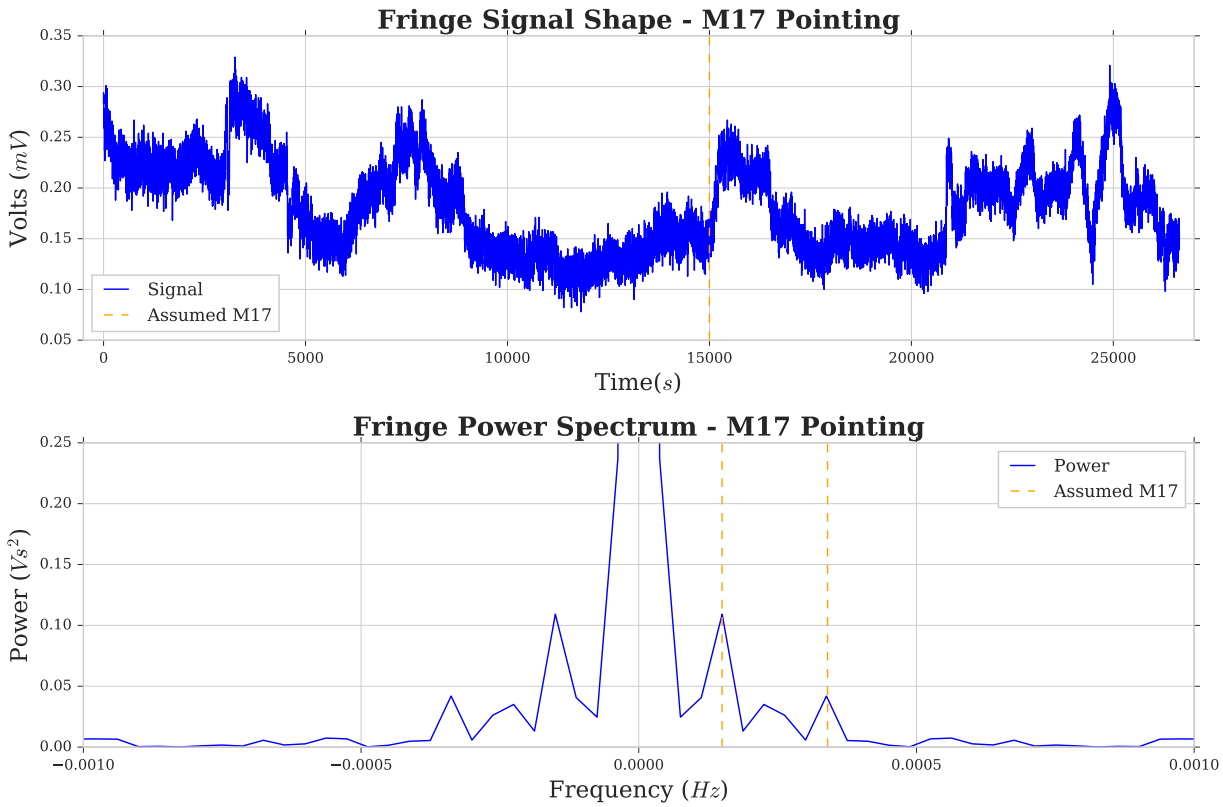

Figure 2: This figure shows our observation of M17. The top graph illustrates the signal produced by the fringe response to a point source, and the bottom graph illustrates the power spectrum associated with the signal. We have inserted dotted lines at where we suspect M17 to be. We chose these points in time due to the unique nature of the source, where it disobeys the overall fluctuation of the signal. This implies that the remaining portions of the signal are observation of the ISM.

3.3.1 Errors in M17 Data

As was not expected, our data collection of M17 was much more precise. Unlike with the Sun, with M17 we were able to complete a full observation. Using the same methods mentioned above in section 3.2.1, our standard deviation came out to be 0.01 mV, or to the nearest $\frac{1}{100}^{th}$ of a mV. This was rather odd since we were unsure if M17 was even present in our data. Our guess is that the smaller deviation came as a result of having a larger amount of data, a common statistical occurrence illustrated in Figure 3 below.

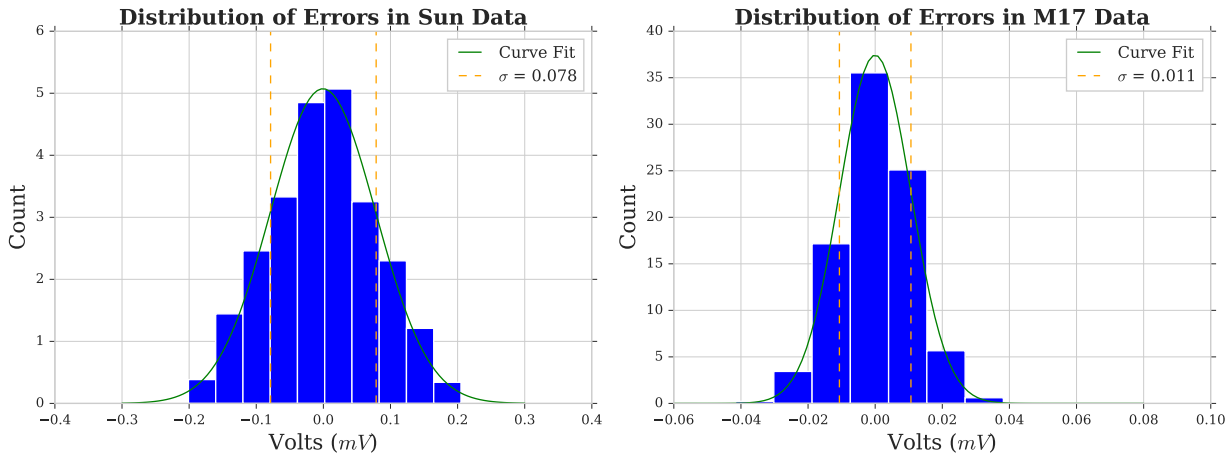

Figure 3: This figure shows the error distributions associated with our observations. The elements of the graphs include a normalized histogram distribution, a function fitted to the histogram, and a dotted line that represents one standard deviation from the mean. According to the figure, our observation of M17 demonstrated a much smaller distribution of values, indicating either that our source was captured or that our data was similar to that of a large, fairly consistent sample size. We found $\sigma_{Sun} = 0.078$ and $\sigma_{M17} = 0.011$.

4 Data Analysis

4.1 Calculating Baselines

Determining the baselines was crucial in resolving the local fringe amplitudes of our signal. It is important to note that rather than working through the baseline values directly, we used Equations 3 and 4, and developed a list of guesses for both Q_{ew} and Q_{ns}, setting $B_{ew} = 16$ and $B_{ns} = 1$ as our expected values. We expanded our list of Q values about that of the expected Q value and iterated over the list, inputing each of our values into Equation 1. We then applied the *curvefit* module which uses a non-linear least squares to fit a function, f, to our data. The inputs were our fringe amplitudes gathered from Equation 1 and our original Sun 'Volts' data. This made it possible to solve for parameters A and B, which were then used to solve Equation 1.

These solutions were compiled into an array and used to calculate the sum of the residuals squared between our solutions and the original data. These values, noted as S, were put into a 10x10 matrix, representing our 10 guesses for both Q_{ew} and Q_{ns}. We concluded that the minimum S value corresponded to the most precise values for Q. This process was done for both sources. Our Sun data showed $B_{ew} \approx 16.54$ meters and $B_{ns} \approx 0.97$ meters, with a full baseline $B \approx 16.57$. Our M17 data showed $B_{ew} \approx 17.19$ meters and $B_{ns} \approx 1.01$ meters, with a full baseline $B \approx 17.22$.

4.1.1 Local Fringe Frequencies

The local fringe frequencies were solved for using Equation 5. Substituting in our best values for Q, we set $Q_{ew} = 661.11$ and $Q_{ns} = 23.88$. Below is the docstring of the function we defined to calculate the local fringe frequencies. For our Sun data, the minimum fringe frequency of 0.01 Hz corresponded to a local minimum in the fringe's power spectrum at about the same frequency, indicating that our range of fringe frequencies was correct.

```
def fringe_freqs(hours, volts):
    '''Return a list of the local fringe frequencies.
    Parameters
    ----------
    hours : hour angle array
    volts : sampled data

    Returns
    -------
    F_freqs : list of the local fringe frequencies'''
```

4.1.2 Errors in Q Values

The errors associated with the measurement of the baseline components were solved for by inverting our covariance matrices. The *curvefit* module did us the favor of returning both parameter values A and B, and their respective covariance values in a 2x2 matrix. Reading further into the module, we learned that the errors could be extrapolated by taking the square root of the diagonal of our covariance matrix. We then compiled these values into a list and used the same method of implementing histograms as mentioned earlier. Though not as bell-shaped as the other distributions, this distribution of baseline component errors shown in Figure 4 measured a standard deviation much less than 1% at an impressive 2.76×10^{-7}. This suggests that we measured our baseline components with a precision just less than one-millionth of a percent.

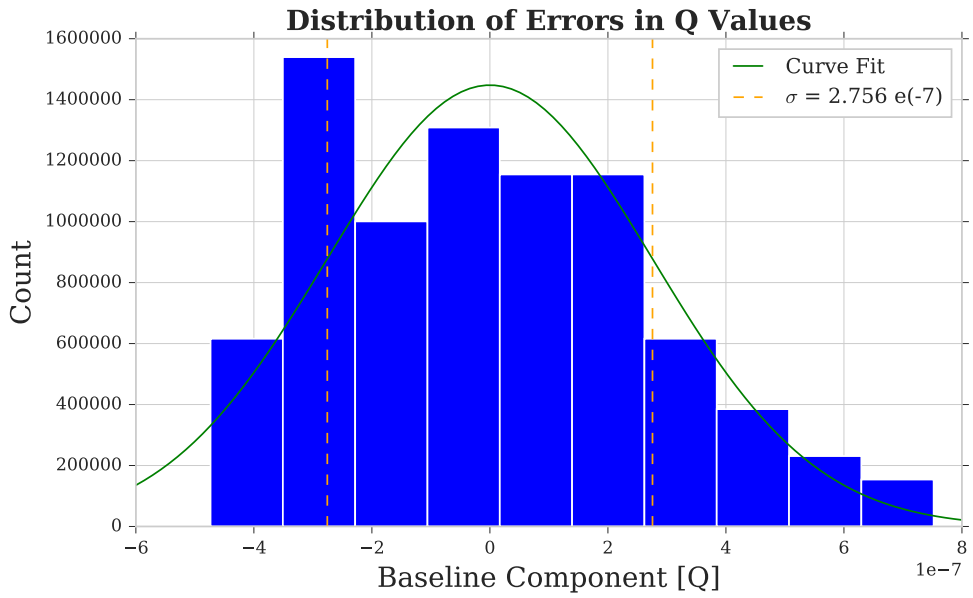

Figure 4: This figure shows the distribution of values for the baseline component. The elements of the graph include a normalized histogram distribution, a function fitted to the histogram, and a dotted line that represents one standard deviation from the mean. Looking at this graph, we realized that the values for our baseline component were not quite evenly distributed. This indicated the presence of a smaller deviation which we happened to measure as $\sigma_{Sun} = 2.756 \times 10^{-7}$.

4.2 Measuring the Diameter of the Sun

To measure the diameter of the Sun, we first had to define a modulating function that allowed us to sift through the information of our signal. One function in particular that allowed us to do so, was the Bessel function $j1$ from the *scipy.special* module. The reason we assumed a Bessel function was because it was the only function we knew that displayed the fluctuating characteristics of our fringe signal. We knew that the Fourier transform of the source intensity distribution on the sky was expressed by the fringe modulator, and thus could also be expressed by the Bessel function. The roots of our Bessel function, expressed here as x_n, could be used to extrapolate the angular diameter of the Sun like so:

$$u = \frac{B}{\lambda} cos(h_{s,0}) \longrightarrow \Theta_r = \frac{x_n}{2\pi u} \tag{6}$$

Setting B as our total baseline and $\lambda = 2.5$ cm, we used the average value of our hour angles to compute the expression for u. Plugging this into the equation for Θ_r, we iterated over the entire list of roots for $j1$ and filtered out the angular diameters above 0.3°and below 0.2°. We calculated $\Theta_r = 0.289°$ for the Sun, a value that deviated 15.6% from our expected value of about 0.25°.

4.2.1 Using Angular Diameter to Solve for Circular Diameter

To check our answer for Θ_r, we went ahead and used simple trigonometry to solve for the circular diameter of the Sun and compared it to its actual value hoping for a smaller margin of error. Taking the product of

the angular diameter with the distance of the Sun from Earth, we were able to calculate a solar diameter of about 7.6×10^8 m, only 8.6% shy of the expected diameter of 7.0×10^8 m.

5 Conclusion

Despite not having a complete observation of the Sun, the data proved to be promising. We were able to measure the diameter of the Sun within 9% of its true value, suggesting that a longer observation would have only provided us with a more precise measurement. Additionally, both sources returned full baseline values that differed by just under 3%. This assured us that our measurements for the baseline components were precise enough so as to yield the most accurate diameter of the Sun. Our biggest concern were the counts associated with error distribution in Figure 4. Having established lists of length 100 that contained our A and B error values, we were puzzled to find that the distribution of errors had values that counted in the millions. The only explanation we could conjure up was that the dot product of our two lists returned a 100x100 matrix, but even this falls short of the counts by two orders of magnitude.

5.1 Contributions

Arthur and Oscar contributed the most to developing our pointing and data acquisition scripts, though slightly edited from that which was provided by the lab. I worked alone on the remaining plots and data calculations presented throughout the report.